

Simulating the Response of a Composite Honeycomb Energy Absorber: Part 1. Dynamic Crushing of Components and Multi-Terrain Impacts

K. Jackson¹, E. Fasanella², and M. Polanco³

¹NASA Langley Research Center, Mail Stop 495, 12 West Bush Road, Hampton, VA 23681-2199; Ph (757) 864-4147; email: karen.e.jackson-1@nasa.gov

²National Institute of Aerospace, Mail Stop 495, NASA Langley Research Center, Hampton, VA 23681-2199; Ph (757) 864-4345; email: edwin.l.fasanella@nasa.gov

³ATK Space Systems, Inc., Mail Stop 495, NASA Langley Research Center, Hampton, VA 23681-2199; Ph (757) 864-3992; email: michael.a.polanco@nasa.gov

ABSTRACT

This paper describes the experimental and analytical evaluation of an externally deployable composite honeycomb structure that is designed to attenuate impact energy during helicopter crashes. The concept, designated the Deployable Energy Absorber (DEA), utilizes an expandable Kevlar® honeycomb to dissipate kinetic energy through crushing. The DEA incorporates a unique flexible hinge design that allows the honeycomb to be packaged and stowed until needed for deployment. Experimental evaluation of the DEA included dynamic crush tests of multi-cell components and vertical drop tests of a composite fuselage section, retrofitted with DEA blocks, onto multi-terrain. Finite element models of the test articles were developed and simulations were performed using the transient dynamic code, LS-DYNA®. In each simulation, the DEA was represented using shell elements assigned two different material properties: Mat 24, an isotropic piecewise linear plasticity model, and Mat 58, a continuum damage mechanics model used to represent laminated composite fabrics. DEA model development and test-analysis comparisons are presented.

INTRODUCTION

Since its inception in 2006, the NASA Subsonic Rotary Wing (SRW) Aeronautics Program in Rotorcraft Crashworthiness has focused attention on two areas of research: the evaluation of an externally deployable energy absorbing (DEA) concept and improved prediction of rotorcraft crashworthiness (Jackson, 2009). The DEA is a composite honeycomb structure that can be deployed, much like an external airbag system, to provide external energy attenuation (Kellas, 2007). The concept was originally proposed and studied as a passive energy attenuation system for the Orion crew module, and was designed to significantly reduce impact loads transmitted to the crew during land or water impact following capsule re-entry. Eventually, the Orion Program Office focused on other energy attenuating concepts that had higher technical maturity (Vassilakos, 2011). However, during this early evaluation, the DEA concept demonstrated excellent energy absorption capabilities. As a result, the

SRW Program selected the concept for further evaluation. Pre- and post-test photographs of a sample DEA component are shown in Figure 1.

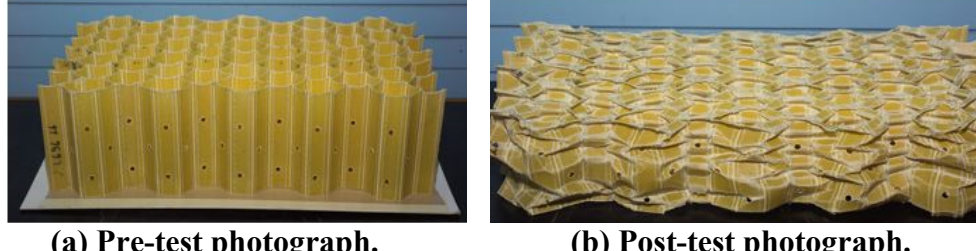


Figure 1. Pre- and post-test photographs of a sample DEA component.

The DEA is an expandable honeycomb structure designed to absorb impact energy by crushing, which is achieved through local cell wall bending, plastic hinge formation, and minor tearing, as shown in Figure 2. Unlike other cellular energy absorbers in use today, the DEA utilizes a unique and patented flexible hinge at each junction of its cell walls (Kellas, 2004). This feature enables the energy absorber to be fabricated and readily deployed either radially (omnidirectional energy absorption) or linearly (unidirectional energy absorption). Like conventional honeycomb, once expanded the energy absorber is transformed into an efficient orthotropic cellular structure, with greater stiffness and strength along the cell axis as compared to the transverse directions.



Figure 2. Close-up photograph of the crushing modes exhibited by the DEA.

Experimental evaluation of the DEA utilized a building block approach that included material characterization testing of its constituent, Kevlar®-129 fabric/epoxy; flexural testing of single hexagonal cells; dynamic crush tests of multi-cell components; and vertical drop tests of a composite fuselage section, retrofitted with DEA blocks, onto concrete, water, and soft soil (Kellas, 2007 and Kellas, 2008). As a final demonstration, a full-scale crash test of an MD-500 helicopter, retrofitted with DEA blocks, was conducted in December 2009 at NASA Langley Research Center (Kellas, 2010 and Littell, 2010). During each stage of the DEA evaluation process, finite element models of the test articles were developed and simulations were performed

using the explicit, nonlinear transient dynamic finite element code, LS-DYNA® (Hallquist, 2006).

The objectives of this paper are to document the results of analytical simulations that were performed during evaluation of the DEA concept. Specifically, this paper will focus on simulations of dynamic crushing of multi-cell DEA components and vertical drop tests of a composite fuselage section, retrofitted with DEA blocks, onto three different terrains. The performance of two specific material models were evaluated in shell-element-based models of the DEA including Mat 24, an isotropic piecewise linear plasticity model, and Mat 58, a continuum damage mechanics based model used to simulate laminated composite fabrics.

MATERIAL MODEL DEVELOPMENT

A major challenge in developing a reliable and robust shell-based model of the DEA is to generate an accurate material model to represent Kevlar®-129 fabric/epoxy. The use of shell elements in modeling the thin composite honeycomb provides for a more realistic representation of the DEA geometry than can be generated using solid elements. In addition, property diminishment of individual plies can be implemented based on damage mechanics models. However, modeling of composites has long been complicated by the variety of failure modes they exhibit under compression, such as local buckling, delamination, and tearing. These interacting failure modes can complicate the ability to simulate the crush response of the DEA under load. To accurately characterize Kevlar®-129 fabric/epoxy, an LS-DYNA® material model was needed with the capability to predict the observed failure mechanisms in the DEA and to demonstrate good functionality when used in conjunction with a shell-element-based model. Two materials (Hallquist, 2006) were investigated: Mat 58, or *MAT_LAMINATED_COMPOSITE_FABRIC, and Mat 24 or *MAT_PIECEWISE_LINEAR_PLASTICITY.

Mat 58 Laminated Composite Fabric Material Model

The Mat 58 material model was initially chosen as a result of past success in predicting debris impact damage to the Reinforced Carbon-Carbon leading edge panels of the Space Shuttle Columbia (Carney, 2004 and Fasanella, 2006). Mat 58 is a continuum damage mechanics material model based on the theory by Matzenmiller (1995) and is intended for use with shell elements to simulate composite tape laminates and woven fabrics. Schweizerhof (1998) describes the implementation of Mat 58 within LS-DYNA®. The model requires input of material properties in tension, compression, and shear to define stress-strain behavior within the lamina or laminate. The user specifies the in-plane elastic modulus and Poisson's ratio in two primary directions, designated A (typically used for the longitudinal or fiber direction) and B (typically used for the transverse or perpendicular-to-the-fiber direction) in LS-DYNA®. The maximum strength in tension, compression, and shear is also specified at corresponding strain values. A representation of the stress-strain curve for in-plane tension is illustrated in Figure 3. The tensile response is initially linear elastic with the modulus specified by EA. Stress increases nonlinearly until

XT, the maximum strength, is reached. The nonlinear portion of the response is defined internally by LS-DYNA® based on a continuum damage approach. Once XT is reached, the stress is reduced based on the “stress limiting” factor SLIMT1, and is then held constant at the reduced value until elements reach a strain specified by the ERODS parameter in the material model, at which point the elements are deleted and removed from the solution. Similar stress-strain responses are defined for in-plane compression and shear.

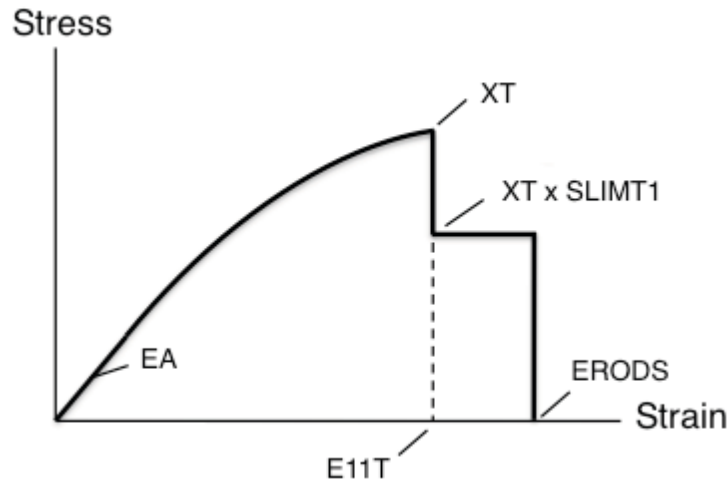


Figure 3. Typical in-plane tension stress-strain curve used in Mat 58.

Initial input parameters for Mat 58 were determined based on data obtained from tensile tests conducted on single-ply Kevlar®-129 fabric/epoxy coupons oriented at 0°/90° and ±45° with respect to the loading axis, as reported in Kellas (2007). Tensile properties for the model were obtained from 0°/90° tensile data while shear properties were obtained from ±45° tensile coupon tests. As described in Polanco (2009), Mat 58 was superior to Mat 24 in predicting the 3-point bending response of single hexagonal cells fabricated of Kevlar®-129 fabric/epoxy. However, the same Mat 58 model performed poorly in predicting the crushing response of DEA components (Polanco, 2009). The value of compressive strength used in the previous Mat 58 model was found to be excessively high at over 60,000-psi along the fiber direction (Fasanella, 2012).

Updated Mat 58 properties used in the current modeling effort are listed in Table 1. Note that since the Kevlar® material used to construct the DEA is a plain weave fabric, the modulus in the longitudinal or fiber direction (EA) is the same as the modulus for the transverse direction (EB). The Mat 58 material property also requires input of the Poisson’s ratio in the BA direction, as opposed to the more standard AB direction. The Poisson’s ratio in the BA direction can be derived from the ratio of EB to EA multiplied by the Poisson’s ratio in the AB direction. However, since EA=EB, the two values of Poisson’s ratio are the same. Typically, compressive strengths of Kevlar® materials are considerably lower than their corresponding tensile strengths. Aird (2006) states that “when a laminate using Kevlar® reinforcement is loaded in compression...the individual fibrils buckle and split away from the bundle

when the stress exceeds about one-fifth of what it would take in tension.” Since no compressive testing was performed, a range of compressive strength values from 7,500- to 16,000-psi was considered. The low value of compressive strength (7,500-psi) was based on the approximate yield stress of the $\pm 45^\circ$ coupons, while the high value (16,000-psi) was based on 1/5 the tensile strength of 80,000-psi for the $0^\circ/90^\circ$ data. With Mat 58, compressive crush strengths in both the A and B directions of 10,000-psi provided the best fit to data from both the static single cell bending tests and the dynamic DEA component crush tests.

Table 1. Mat 58 material properties used to represent the Kevlar®-129 fabric.

Material Property Description	Symbol	Values
Density, lb-s ² /in ⁴	RO	1.29E-4
Young’s modulus longitudinal & transverse direction, psi	EA, EB	1.3E+6
Poisson’s ratio	PRBA	0.3
Stress limit of nonlinear portion of shear curve, psi	TAU1	Not used
Strain limit of nonlinear portion of shear curve, in/in	GAMMA1	Not used
Shear modulus AB, BC, and CA, psi	GAB	1.54E+5
Min stress factor for limit after max stress (fiber tension)	SLIMT1	0.8
Min stress factor for limit after max stress (fiber comp)	SLIMC1	1.0
Min stress factor for limit after max stress (matrix ten)	SLIMT2	0.8
Min stress factor for limit after max stress (matrix comp)	SLIMC2	1.0
Min stress factor for limit after max stress (shear)	SLIMS	1.0
Material axes option (model dependent)	AOPT	
Maximum effective strain for element layer failure	ERODS	10.0
Failure surface type	FS	1.0
Strain at longitudinal compressive strength, in/in	E11C	0.02
Strain at longitudinal tensile strength, in/in	E11T	0.05
Strain at transverse compressive strength, in/in	E22C	0.02
Strain at transverse tensile strength, in/in	E22T	0.05
Strain at shear strength, in/in	GMS	0.02
Longitudinal and transverse compressive strength, psi	XC, YC	10,000.
Longitudinal and transverse tensile strength, psi	XT, YT	80,000.
Shear strength, psi	SC	5,000.

Piecewise Linear Plasticity Material Model

Due to initial difficulty in characterizing the DEA material response, a less complex material model was sought to represent Kevlar®-129 fabric/epoxy. Thus, Mat 24, known as *MAT_PIECEWISE_LINEAR_PLASTICITY (Hallquist, 2006), was chosen and used in prior simulations of the DEA (Polanco, 2009). In the model, the user can specify the elastic modulus, Poisson’s ratio, yield stress, and tangent modulus of the material. The user can also input an effective stress versus effective plastic strain curve that defines the isotropic material response. Material property values used in Mat 24 to represent Kevlar®-129 fabric/epoxy are listed in Table 2 and the input stress-strain curve, which was based on the average tensile responses of $\pm 45^\circ$ coupons, is shown in Figure 4. It should be noted that the tangent modulus listed in Table 2 was set to zero in this case, indicating that the plastic response of the

material was defined by the input stress-strain curve. Finally, the compressive response was assumed to be equivalent to the tensile response for the initial portion of the curve, since no compressive test data were obtained.

Table 2. Property values used in Mat 24.

Parameter	Symbol	Description	Value
1	E (psi)	Young's modulus	340,000
2	PRBA	Poisson's Ratio	0.3
3	SIGY (psi)	Yield stress	7,500
4	ETAN (psi)	Tangent modulus	0

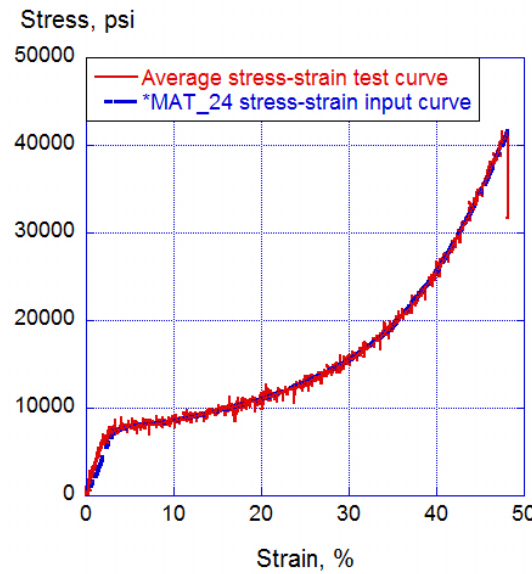


Figure 4. User-defined stress-strain input curve for Mat 24.

DEA COMPONENT CRUSH TESTING AND SIMULATION

Three multi-cell components were tested to evaluate the energy absorption capabilities of the DEA under both normal and off-axis loading conditions (Kellas, 2007). Each of the components was fabricated of multiple hexagonal cells having a 1-in. flat facet width and constructed of 1 or 2 layers of Kevlar®-129 fabric/epoxy, oriented at $\pm 45^\circ$ with respect to the longitudinal axes of the cells. This configuration of the DEA was designed to provide an average crush stress of 20-psi. Two of the DEA components, consisting of 59- and 104-cells, were manufactured such that the longitudinal axes of the cells were oriented in the same direction as loading (normal). A third DEA component, consisting of 68-cells, was fabricated such that the longitudinal axis of the cells was canted by 27° with respect to the direction of loading (off-axis). The top surface of each DEA component was curved slightly to reduce the high peak loads that can occur during initial impact. Also, transverse holes were drilled into the DEA components to allow entrapped air to escape. Each component was impacted in a fully deployed state by a rigid impact mass, or block, that translated on vertical support rods through low-friction bearings. The drop mass was instrumented with

an accelerometer to record the vertical acceleration response. Dimensions of each DEA component and the impact test conditions are listed in Table 3.

Table 3. Details of DEA Component Crush Testing.

Number of cells	Cell orientation*	Length, in.	Width, in.	Height, in.	Weight of impact block, lb.	Impact Velocity, in/s
59	0°	16	12.4	6.0	412.5	195.6
104	0°	21	15.8	10.0	477.2	266.4
68	27°	16	14.0	6.7	477.2	183.6

*with respect to the vertical, or loading, direction

Dynamic crush tests of multi-cell DEA components were simulated in LS-DYNA® using Mat 58 and Mat 24 to represent the Kevlar®-129 fabric/epoxy. Shell-element-based models were developed to represent the normal (59- and 104-cell) and off-axis (68-cell) DEA components, as shown in Figure 5. All models consisted of four parts, including an impact block used to crush the DEA, a reaction surface placed under the honeycomb, one part for plies within the DEA having a thickness of 0.01-in., and another part for double plies with a thickness of 0.02-in. The *SECTION_SHELL and *INTEGRATION_SHELL cards were used with Mat 58 to specify the ±45° ply orientations of the cell walls.

For each simulation, the impact blocks were assigned a vertical impact velocity to match the test conditions, which are listed in Table 3. Gravitational loading was included in all models. An automatic contact definition was used to represent contact between the impact block and the DEA, between the DEA and the reaction surface, and for internal contact between elements within the DEA. A coefficient of friction of 0.35 was specified in the contact definition. All nodes on the impact surface were fully constrained and the impact surface and impact block were both modeled as *MAT_RIGID in LS-DYNA®. The nominal edge length of the shell elements used to create the DEA models was 0.25 inches. Information on all three DEA component models is listed in Table 4.

Prior to presenting the test-analysis results, it is important to specify the calibration metrics used to assess the level of agreement. For the dynamic crush tests of the DEA components, test-analysis comparisons are presented for four parameters: initial peak acceleration, average acceleration over a specified time duration, average crush stress, and peak compaction acceleration. Note that the average crush stress is determined by adding 1 to the average acceleration to account for gravitational loading, then multiplying the sum by the weight of the impact block and dividing by the impacted area of the DEA. In addition, plots showing unfiltered test and unfiltered predicted acceleration time history responses are provided. These metrics were selected based on the stated design goal for the DEA. The level of agreement between test and analysis is evaluated based on a simple percentage difference approach, where agreement with ±15% is considered good.

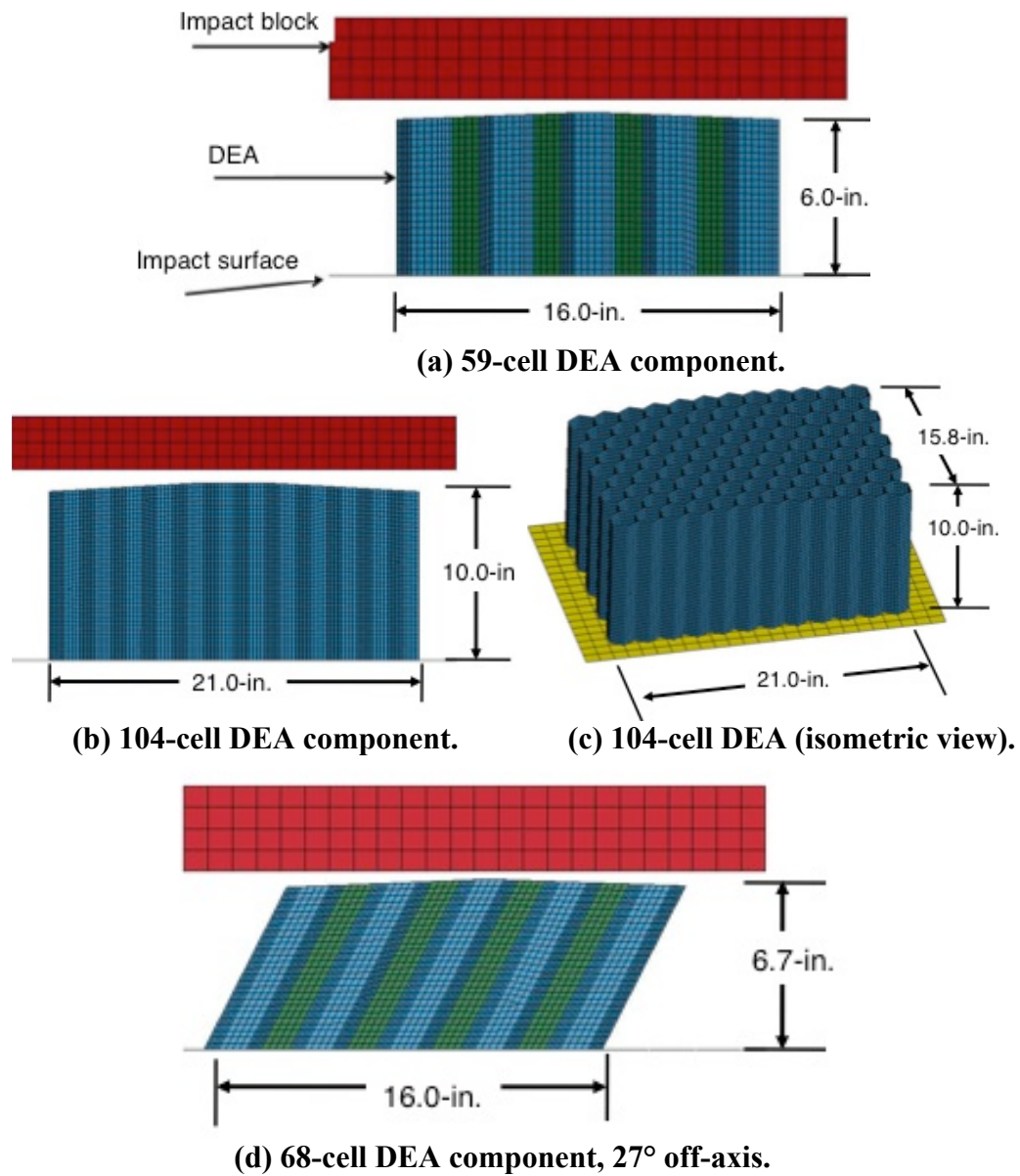


Figure 5. Pictures of the shell element DEA component models.

Table 4. Multi-Cell DEA component model information.

Property	59-Cell	104-Cell	68-Cell
Number of nodes	22,161	53,329	27,435
Number of solid elements	1,920	2,240	1,920
Number of shell elements	20,096	56,052	25,515
Number of parts	4	4	4
Number of Linux-based processors	4	4	4
Approximate run time, minutes	19	87	22
Termination time, s	0.06	0.06	0.1

Results for the 59-Cell DEA Component Test

Both Mat 58 and Mat 24 material models were used to represent the Kevlar®-129 fabric/epoxy cell walls in the shell-based model of the 59-cell DEA crush test. The material properties listed in Table 1 were used for Mat 58, while the material properties listed in Table 2 were assigned to Mat 24. A plot of experimental and predicted acceleration time history responses are shown in Figure 6 and correlation metrics are listed in Table 5. The acceleration response of the model with Mat 58 properties closely follows the test data up to 0.0175-seconds. The predicted acceleration response then exceeds the test data by about 2-3 g's for 0.015-seconds, which slowed the impact block enough to make the predicted compaction peak only 30-g as compared to 64.4-g for the test. In comparison, the model that was executed with Mat 24 accurately predicted the initial peak acceleration and the uniform crush response up to 0.015-seconds. Subsequently, the predicted acceleration increases and demonstrates a compaction response. The magnitude of the predicted compaction peak was under predicted (27.4-g for the model compared with 64.4-g for the test) and the timing of the predicted peak occurred earlier than the test. As listed in Table 5, the Mat 58 model generally showed better agreement with the test than did Mat 24, though neither model predicted the peak compaction acceleration well.

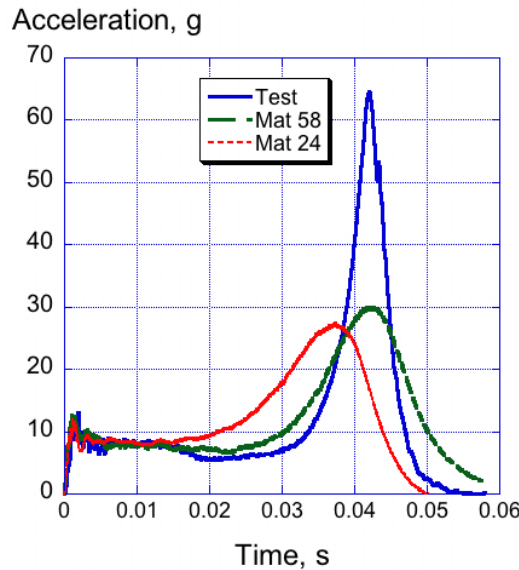


Figure 6. Test-analysis comparisons of the 59-cell DEA component.

Table 5. Test-Analysis Correlation for the 59-Cell DEA Component Models.

Parameter	Test	Mat 24		Mat 58	
		Value	Percentage Difference	Value	Percentage Difference
Initial peak accel., g	12.4	12.2	1.6	13.7	-10.5
*Avg. acceleration, g	7.1	9.7	-36.6	7.8	-9.9
Avg. crush stress, psi	16.9	22.3	-32.0	18.3	-8.3
Compaction peak, g	64.4	27.4	57.5	30.0	53.4

* Average acceleration computed over time interval of 0.0-0.03 seconds.

Results for the 104-Cell DEA Component Test

As with the 59-cell DEA component, both material models (Mat 58 and Mat 24) were used to represent the Kevlar®-129 fabric/epoxy cell walls in the shell-based model of the 104-cell DEA crush test. Experimental and predicted acceleration time history responses are plotted in Figure 7 and correlation metrics are listed in Table 6. The model with Mat 58 properties under predicts the initial acceleration, but predicts the uniform crush response within 12%, and even predicts the unloading slope at the end of the simulation. Likewise, the model with Mat 24 material properties under predicts the initial peak acceleration, but predicts the uniform crush response within 10% of the test data. However, this model also predicted a compaction acceleration starting at 0.035-s that is not present in the test data.

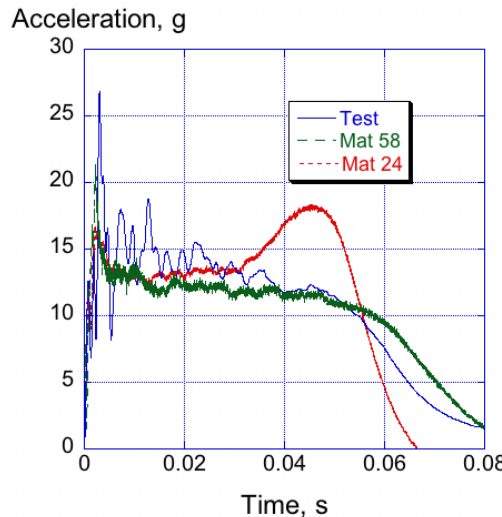


Figure 7. Test-analysis comparisons of the 104-cell DEA component.

Table 6. Test-analysis correlation for the 104-cell DEA component models.

Parameter	Test	Mat 24		Mat 58	
		Value	Percentage Difference	Value	Percentage Difference
Initial peak accel., g	26.8	16.8	37.3	21.3	20.5
*Avg. acceleration, g	14.3	13.0	9.1	12.7	11.2
Avg. crush stress, psi	22.1	20.2	8.6	19.8	10.4
Compaction peak, g	-	18.0	-	-	-

* Average acceleration computed over time interval of 0.0-0.03 seconds.

The correlation metrics listed in Table 6 indicate that the Mat 58 model predicts the initial peak acceleration better than the Mat 24 model. However, over the first 0.03 seconds, the average acceleration of the Mat 24 model (13.0-g) is closer to the test average of 14.3-g and the predicted average crush stress is also closer to the test (20.2-psi for the model compared with 22.1-psi for the test). After 0.03 seconds, the Mat 24 model deviates from the test data and shows a compaction peak, while the Mat 58 response remains closer to the test data. Thus, visual

inspection of the test-analysis comparison plot is as important, in this case, as the individual correlation metrics in evaluating the performance of the material model.

Results for the 68-Cell DEA Component Test

As with the 59- and 104-cell DEA component models, both materials (Mat 58 and Mat 24) were used to represent the Kevlar®-129 fabric/epoxy cell walls in the shell-based model of the 68-cell canted DEA crush test. Experimental and predicted acceleration time history responses are plotted in Figure 8 and correlation metrics are listed in Table 7. For this simulation, the Mat 58 model matches the initial peak magnitude and the uniform crush response of the test. The acceleration peak at compaction is over predicted by about 6-g (33.9-g versus 27.7-g for the test) and occurs approximately two milliseconds before the test peak occurs. In comparison, the Mat 24 model over predicts the initial peak acceleration by approximately 7-g, but predicts the subsequent reduction in acceleration attributed to outer cell buckling, and the compaction response of the component. The magnitude of the peak acceleration during compaction is slightly over predicted (29.8-g compared with 27.7-g for the test) and the predicted compaction peak occurs earlier in time than the test peak. Early compaction occurs in the simulation with Mat 24 due to global buckling of the cell walls.

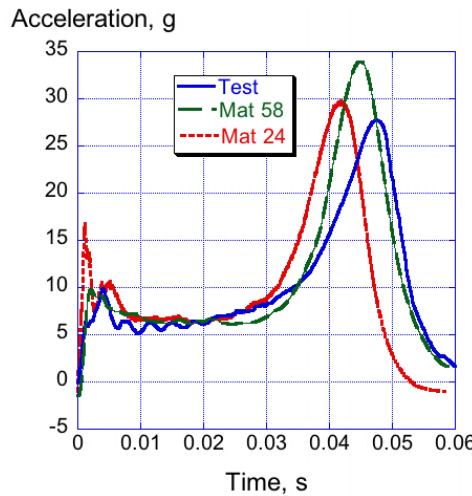


Figure 8. Test-analysis comparisons of the 68-cell DEA component.

Table 7. Test-analysis correlation for the 68-cell DEA component models.

Parameter	Test	Mat 24		Mat 58	
		Value	Percentage Difference	Value	Percentage Difference
Initial peak accel., g	9.9	16.8	-69.7	9.7	2.0
*Avg. acceleration, g	6.5	7.6	-16.9	6.6	-1.5
Avg. crush stress, psi	16.0	18.3	-14.4	16.2	-1.5
Compaction peak, g	27.7	29.8	-7.6	33.9	-22.4

* Average acceleration computed over time interval of 0.0-0.03 seconds.

MULTI-TERRAIN IMPACT TESTING AND SIMULATION

A major challenge that designers face when considering crashworthiness of helicopters arises from the unknown morphology of the crash site, including surfaces such as concrete, water, and soft soil. In fact, helicopter accident data indicate that more than 80% of crashes occur onto multi-terrain surfaces such as water, soft soil, plowed or grassy fields, and shallow swamps, as opposed to smooth prepared surfaces (Baldwin, 2000). In addition, research studies have shown that helicopters, designed for crash resistance onto hard surfaces, do not perform well during multi-terrain impacts (Sareen, 2002; Fasanella, 2007; Witlin, 1997; Tho, 2004; Kohlgruber, 2004; and Pentecote, 2002). For hard and non-yielding impact surfaces, the vehicle's kinetic energy has to be managed by the airframe and internal and/or external energy absorbing devices to ensure load attenuation and adequate post-crash cabin volume. Often, legacy airframes have little or no internal structure designed for crash energy management. Consequently, external energy absorbers with large stroke capability are often needed.

The successful utilization of the deployable honeycomb in multi-terrain impact applications requires the capability to transfer load from the impact surface into the cell walls to initiate progressive crushing. Essentially, for soft surface and water impacts, the honeycomb must be prevented from acting as a "cookie cutter". Therefore, the honeycomb's bottom surface, which contacts the impact medium, must be covered, as illustrated in Figure 9. While the primary role of a cover is to introduce the load into the honeycomb cells, the cover also has to be geometrically compatible with the energy absorber, both in its stowed and deployed stages. Several energy absorber cover concepts were considered and the ones that met all design requirements for vertical impacts were fabricated and tested, as described in Kellas (2008).

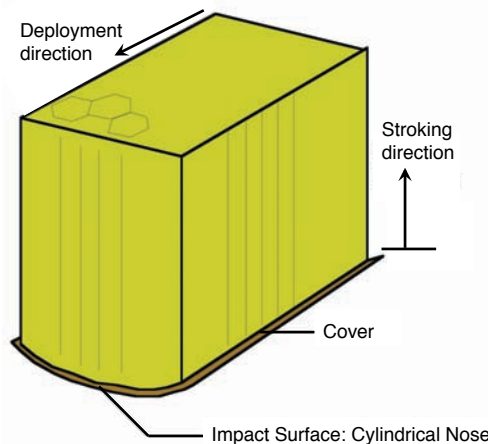


Figure 9. Schematic of a covered deployed energy absorber.

In 2006 and 2007, vertical drop tests were conducted using a 5-ft-diameter, 5-ft-long composite fuselage section to evaluate the energy absorption capabilities of

the DEA during multi-terrain impact. In particular, tests were performed onto a rigid concrete surface, water, and soft soil (sand). The composite fuselage section was developed during a prior research program (Jackson, 2001) at NASA Langley Research Center and was used as a test bed to evaluate the responses of seats and dummies (Fasanella, 2004), to study quantitative correlation methods including experimental uncertainty (Lyle, 2002), and to examine the influence of multi-terrain (Fasanella, 2007). The fuselage section is fabricated using composite sandwich construction and details of its design can be found in Jackson (2001).

For the multi-terrain impact tests that were conducted as part of the DEA evaluation program, the fuselage section was outfitted with ten 100-lb lead blocks that were mounted, five per side, to the floor of the fuselage section using standard seat rail fasteners. Accelerometers were mounted on the lead blocks to record the dynamic structural response of the floor. Four DEA blocks were fabricated and attached to the bottom surface of the fuselage section. The DEA blocks were made of one or two plies of Kevlar®-129 fabric/epoxy, oriented at $\pm 45^\circ$ with respect to the longitudinal cell-wall direction, had a nominal cell edge length of 1.0-in., and weighed 5.6-lb each. Thus, the total weight of the test article for each multi-terrain impact test was approximately 1,220-lb. The deployed size of the honeycomb blocks was 20-in. tall, 16.5-in. wide and 20.5-in. deep and incorporated a curved surface (18-in. radius) on the bottom to alleviate the initial peak loads for rigid surface impacts. Each DEA block incorporated a cover consisting of a single woven ply of Kevlar®-129 fabric/epoxy. The DEA blocks were sized based on the rigid-surface impact test with the assumption that the kinetic energy of a 40-ft/s impact would be managed through crushing of the DEAs while restricting average floor-level accelerations to less than 20-g. Therefore, 20-g was the target level for the sustained crushing load, also referred to as the energy absorber design crush load. Photographs of the three multi-terrain impact tests are shown in Figure 10.



Figure 10. Pre-test photographs of the composite fuselage section prior to multi-terrain impact. Impact velocity is listed in the figure captions.

LS-DYNA® models were developed to simulate multi-terrain impacts of the composite fuselage section fitted with the DEA onto concrete, water, and soft soil (sand). Identical finite element models of the fuselage section and DEA were

used in each simulation and only the impact medium was changed. General model information regarding details of the multi-terrain simulations can be found in Table 8. Note that the Kevlar®-129 fabric/epoxy cover was represented using shell elements. The rigid impact surface was represented using shell elements, whereas the water and sand surfaces were represented using solid hexagonal elements. The inner and outer face sheets of the upper fuselage cabin and the DEA components were represented using shell elements. However, the upper cabin foam core and the floor foam core were represented using solid elements. Finally, the seat tracks that were mounted to the floor of the fuselage were represented using beam elements and the ten 100-lb lead masses attached to the seat tracks were represented using concentrated mass elements.

The fuselage model contained 7 different material property definitions in total. The laminate stacking sequences of the multi-layered face sheets were defined using *PART_COMPOSITE to specify the material designations of each ply, ply thicknesses and orientation, and the number of integration points per ply. Shell elements used to represent the DEA blocks were assigned the same Mat 58 and Mat 24 material properties that were used previously to represent the DEA components. The DEA shell elements had a nominal element edge length of 0.5-in. For the multi-terrain impacts, calibration metrics were average accelerations over specified time durations and plots of floor-level acceleration time histories. The selection of these metrics was guided by the stated design goal for the DEA, to limit average floor-level accelerations to 20-g or less. Finally, predicted acceleration results for the multi-terrain simulations were filtered using an SAE CFC 60 low-pass filter (SAE, 1995), while test data is unfiltered.

Table 8. Fuselage section with DEA model information.

Property	Rigid	Sand	Water
Number of nodes	126,500	220,305	202,472
Number of solid elements	14,946	99,618	87,846
Number of shell elements (total)	129,573	128,180	128,180
Number of shell elements (DEA)	116,160	117,792	117,792
Number of beam elements	188	188	188
Number of concentrated mass elements	40	40	40
*MAT_24 run time (4 processors), minutes	271	2366	2797
*MAT_58 run time (4 processors), minutes	250	2153	2675

Results for the Rigid Surface Impact

The finite element model for simulating impact of the composite fuselage section with DEA onto concrete is shown in Figure 11. Nodes forming the concrete impact surface were fixed in the model. The four DEA blocks were attached to the fuselage model using the *TIED_SHELL_EDGE_TO_SURFACE option in LS-DYNA®. An automatic contact algorithm was used to define contact interfaces between the concrete surface and the DEA, in addition to modeling self-contact within element segments of the DEA. An impact velocity of 38.4-ft/s was prescribed to the fuselage section and the DEA blocks. A perfectly

vertical orientation of the fuselage was assumed. Two models were executed, one in which the DEA blocks were assigned Mat 24 and the second with Mat 58. The simulations were executed with double precision using LS-DYNA® version 971 for 0.1-seconds. Execution times are listed in Table 8.

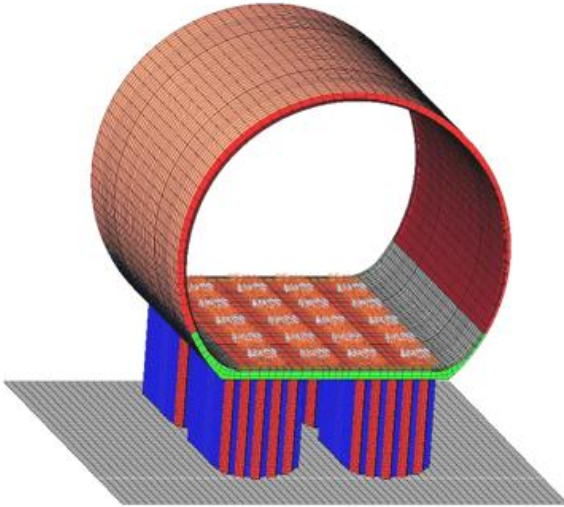


Figure 11. Model of the fuselage section with DEA impacting concrete.

Acceleration time history comparisons, shown in Figure 12, are plotted for the left and right center, left front, and right rear lead blocks on the floor of the fuselage. As a method of judging the level of correlation, average accelerations were obtained for the experimental and analytical responses by calculating the area under the acceleration curves from 0.0- to 0.05-seconds, and then dividing the area by the pulse duration. The values of average acceleration are listed in the plot labels. The Mat 24 responses show a substantial increase in acceleration that occurs between 0.04- and 0.06-s, as a result of DEA compaction. A similar increase is not seen in the test data or in the Mat 58 predicted responses. In general, the Mat 24 responses have shorter duration than either the test data or the Mat 58 responses. The Mat 24 material model predicted an average DEA crush stroke of 13.7-in., while the Mat 58 model predicted the stroke at 14.8-in. Experimental results indicated that the DEA blocks crushed between 14.2- to 14.9-in. based on double integration of measured floor-level acceleration responses.

The average accelerations based on the test data ranged from 18.4- to 19.2-g, indicating a high level of consistency in the test data, with less than 1-g variability based on floor location. In addition, these results show that the design goal for the DEA (to limit average floor-level accelerations to 20-g) was achieved. The Mat 58 predicted average accelerations ranged from 17.1- to 18.2-g, or generally 1-g lower than the test data. Conversely, the Mat 24 predicted average accelerations ranged from 20.2- to 21.0-g, or generally 2-g higher than the test data.

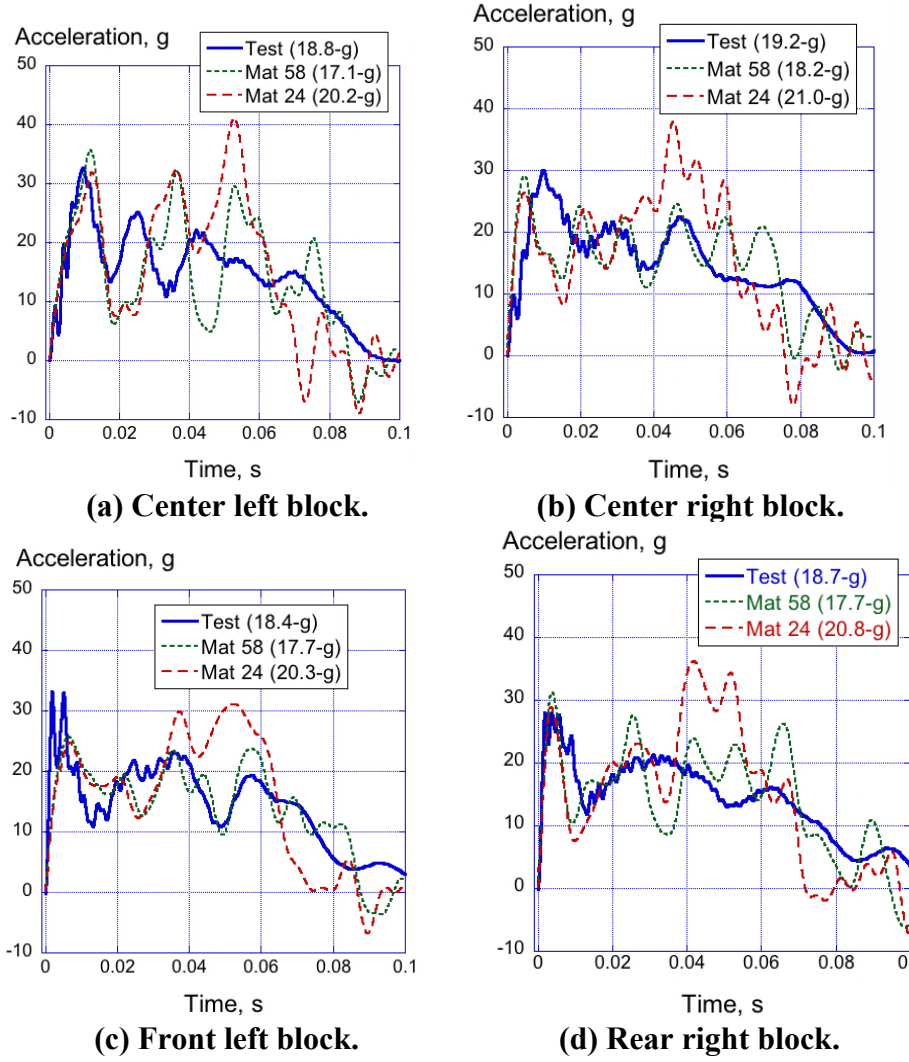


Figure 12. Test-analysis comparisons for the rigid surface impact. Average accelerations are based on a time interval of 0.0- to 0.05-s.

Results for Water Impact

The same fuselage section model used for the rigid surface simulation was also executed for water impact using the Arbitrary Lagrange-Euler (ALE) formulation in LS-DYNA®. The model is shown in Figure 13. Again, two material models were assigned to the DEA, Mat 24 and Mat 58. The water (red mesh) and air (pink mesh) were modeled using 56,700 and 16,200 solid elements, respectively, to simulate the fluid-structure interaction problem. The air region above the water was added to accommodate the splash that occurs upon contact of the water surface with the DEA blocks located beneath the fuselage floor. A perfectly flat attitude of the fuselage was also assumed, and an impact velocity of 27.4-ft/s was prescribed to the fuselage section and DEA blocks. Single-point constraints were applied to the circumference of the water and air meshes in addition to the bottom of the water. The simulations were executed with double precision using LS-DYNA® version 971 for 0.15-seconds.

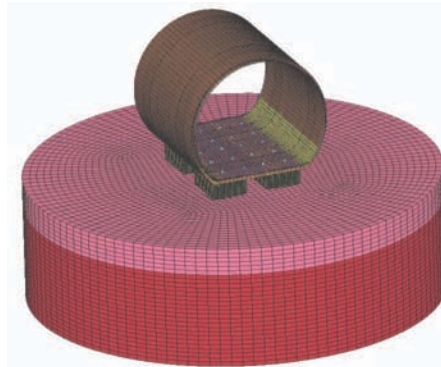


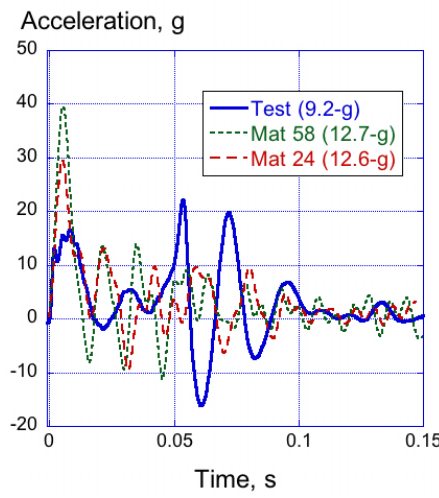
Figure 13. ALE model of the fuselage section with DEA impacting water.

The acceleration responses for both the Mat 24 and Mat 58 material models of the DEA show good qualitative agreement with test data, as indicated in Figure 14. In general, both models over predict the initial peak accelerations of the center lead blocks, but capture the higher initial peaks of the front and rear accelerometers. Neither model predicts the acceleration spikes seen in the center accelerometer locations after 0.05-s that are attributed to impact of the bottom of the fuselage section with the water. Following the water impact test, crushing of the DEA blocks was measured to be less than 1-in. (Kellas, 2008), indicating that energy attenuation occurred through momentum transfer to the water, rather than by crushing of the DEA.

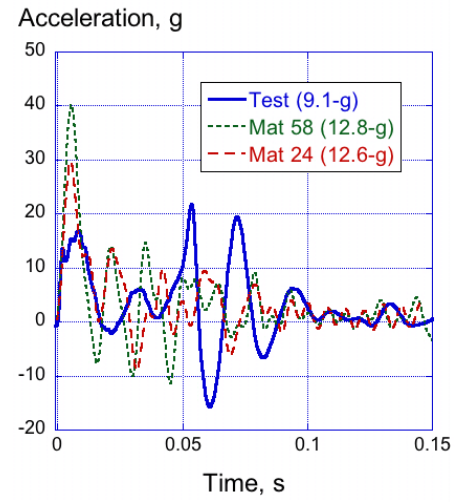
For the water impact, the average accelerations based on the test data ranged from 6.6- to 9.2-g, indicating variability in the test data, based on floor location. Even with the variability, these results show that the design goal for the DEA was achieved. The Mat 58 predicted average accelerations ranged from 12.4- to 12.8-g, and the Mat 24 predicted average accelerations ranged from 12.4- to 12.7-g. These ranges indicate a high degree of uniformity in the predicted floor responses that are not seen in the test data.

Results for Soft Soil (Sand) Impact

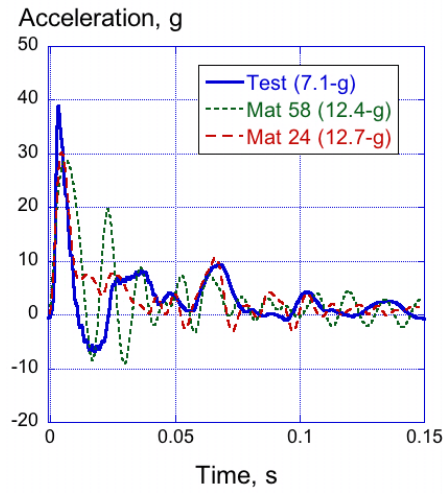
The same fuselage section model that was used during the rigid surface and water impact simulations was also executed for soft-soil impact. The finite element model is shown in Figure 15. The sand was represented by an additional 84,672 solid elements that were assigned Mat 5, *MAT_SOIL_AND_FOAM, material property. Information on the characterization of the sand used in this model can be found in Fasanella (2007, 2008). Like the rigid impact model, the fuselage orientation for sand impact was assumed to be perfectly vertical. Tied contacts were prescribed between the Kevlar[®] cover and the DEA blocks, and between the bottom of the fuselage and the DEA blocks. An automatic contact algorithm was specified to define contact between the sand and the DEA and self-contact within each DEA block. An impact velocity of 37.4-ft/s was prescribed to the fuselage section with the DEA blocks. The simulation was executed with double precision using LS-DYNA[®] version 971 for 0.2-seconds.



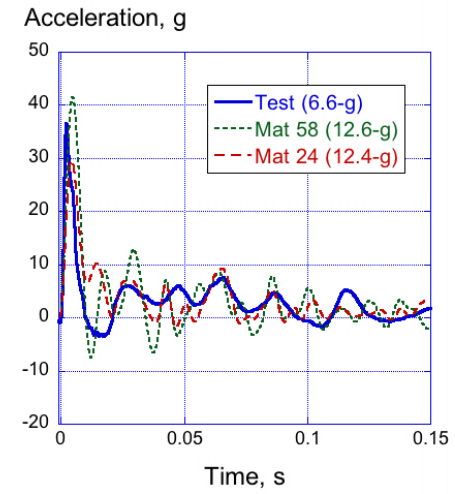
(a) Center left block.



(b) Center right block.



(c) Front left block.



(d) Rear right block.

Figure 14. Acceleration time histories for water impact. Average values are based on a time interval of 0.0- to 0.02-s.

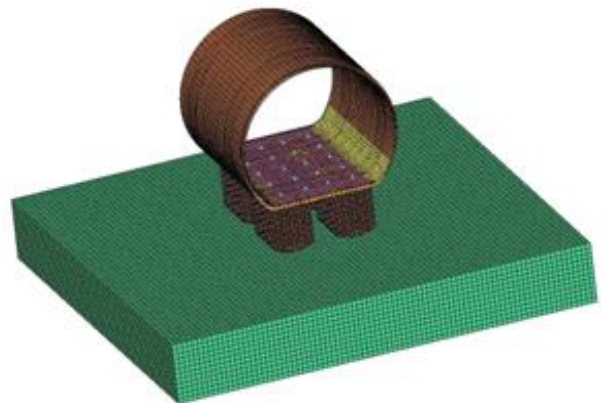


Figure 15. Fuselage section model with DEA components and sand.

In the simulation, the crater depths in the sand ranged between 9- and 10.5-in. for Mat 24 and between 9- and 11-in. for Mat 58, and the crush stroke of each DEA component ranged between 5- and 8-in. for Mat 24 and 3.75- and 5-in. for Mat 58. In the test, between 7- and 9-in. of penetration into the sand was measured, and the amount of DEA crush was estimated to be 6- to 8-in. (Kellas, 2008 and Fasanella, 2008). Acceleration response comparisons from four different floor locations are shown in Figure 16. The plot labels list the average accelerations determined for a time interval of 0.0- to 0.05-seconds. The general analysis trends show good correlation with the test.

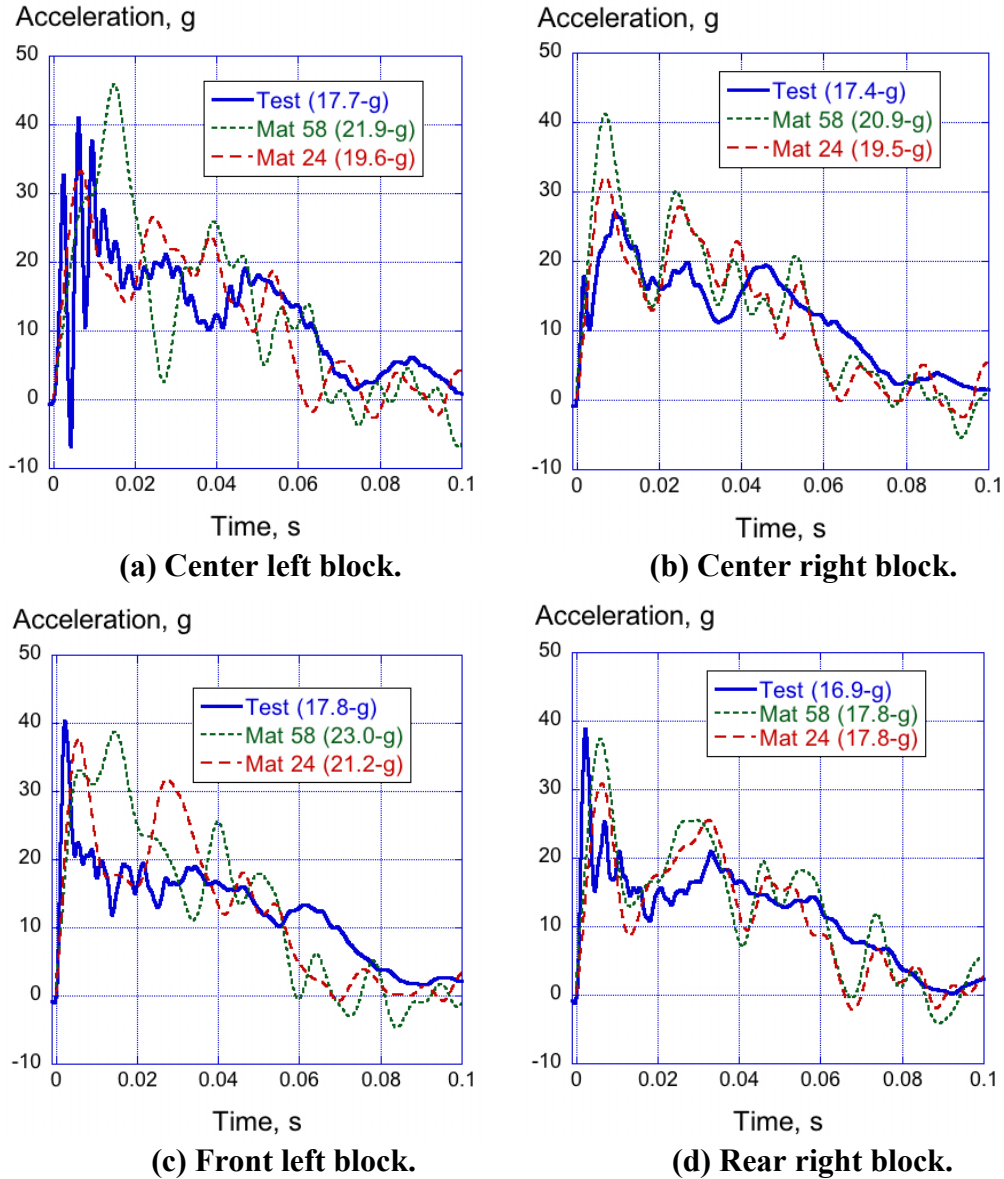


Figure 16. Test-analysis comparisons for sand impact. Average values are based on a time interval of 0.0- to 0.05-s.

For the sand impact, average accelerations based on the test data ranged from 16.9- to 17.8-g, indicating a high degree of consistency in the test data, with less than 1-g variation based on floor location. In addition, these results show that the design goal for the DEA was achieved. The Mat 58 predicted average accelerations ranged from 17.8- to 23-g, and the Mat 24 predicted average accelerations ranged from 17.8- to 21.2-g. These ranges indicate a higher degree of variability in the predicted floor responses than observed in the test data.

DISCUSSION OF RESULTS

The combined loading mechanisms in tension, compression, and shear within the Kevlar[®]-129 fabric/epoxy make it extremely difficult to characterize the crushing response of the DEA. Tension and compression stress-strain responses and strengths are highly dependent on fiber orientation. Consequently, it is difficult to find a single material model that can accurately represent both the linear response to failure of the 0°/90° Kevlar[®]-129 tensile test and the highly nonlinear response of the ±45° Kevlar[®]-129 tensile test, which exhibited matrix failure, scissoring, and high strain-to-failure (Kellas, 2007). Thus, approximations must be made, and the material model chosen will not likely represent all loading conditions equally well. For example, plasticity in compression was simulated in Mat 58 by setting the SLIM parameter to 1. However, strain hardening, if present, must be neglected.

Simple percentage error metrics were selected for four different parameters (initial acceleration, average acceleration during uniform crushing, average crush stress, and compaction peak acceleration) as a means of evaluating the level of correlation achieved by the DEA component simulations. In general, the shell-based models of the DEA components in which Mat 58 was assigned, did a good job of predicting the average crushing behavior within a range of ±15% for all three DEA components. The level of agreement for Mat 24 was more sporadic. For example, the Mat 24 model over predicted the crush response of the 59-cell DEA component by 36%. However, the same material model was able to predict the crushing response of the 104-cell DEA within 10%. For both material models, prediction of the initial and compaction peak accelerations was inconsistent and generally poor. One conclusion that can be drawn is that the simple correlation metrics selected for this simulation study are not adequate to sufficiently assess the test-analysis results. Other metrics that compare both phasing and shapes of experimental and analytical time history responses, such as described by Schwer (2007) and Mongiardini (2009) should be explored.

The DEA was further evaluated during vertical drop tests of a composite fuselage section onto multi-terrain impact (rigid surface, water, and soft soil), in which the design goal was to limit floor-level accelerations to 20-g. Load attenuation through crushing occurred in both rigid surface and soft soil impacts. In these cases, the impact surface provided adequate reaction load to initiate and maintain stable crushing. Given that the impact velocity conditions were nearly identical,

38.4- versus 37.4-ft/s, similar acceleration responses were obtained for these two tests. However, for water impact, kinetic energy was dissipated primarily by accelerating the displaced water volume. Though effective in attenuating the initial peak, the energy absorbers were not able to absorb kinetic energy through crushing (Kellas, 2008). This finding is by no means a drawback of the energy absorber but is simply a reality associated with water impact. For all multi-terrain impact tests, measured average floor-level accelerations were below the 20-g limit, thus the design goal of the energy absorber was achieved.

CONCLUDING REMARKS

An experimental and analytical study was conducted to assess the energy absorption capabilities of a novel Deployable Energy Absorber (DEA). The DEA is a composite honeycomb structure that can be deployed, much like an external airbag system, to provide energy attenuation during aircraft or rotorcraft crash events. A building block approach was taken during the experimental program that included dynamic crushing of multi-cell DEA components subjected to both normal and off-axis loading and vertical drop testing of a composite fuselage section, retrofitted with four DEA blocks, onto multi-terrain surfaces. Finite element models were developed to represent these experiments and simulations were performed using the explicit nonlinear transient dynamic code, LS-DYNA®. The performance of two specific material models were evaluated in shell element based models of the DEA including Mat 24, an isotropic piecewise linear plasticity model, and Mat 58, a continuum damage mechanics based model used to represent laminated composite materials and fabrics.

Dynamic crush tests of three multi-cell DEA components were performed for both normal and off-axis loading. Shell-element models were developed to represent the DEA components and test-analysis comparisons were made to determine if they could accurately predict initial loading, sustained crushing, and compaction responses of the DEA components. In general, the models in which Mat 58 was assigned, did a good job of predicting the average crushing behavior within a range of $\pm 15\%$ for all three DEA components. The level of agreement for Mat 24 was more sporadic. For both material models, prediction of the initial and compaction peak accelerations was inconsistent and generally poor. One conclusion that can be drawn is that the simple correlation metrics selected for this simulation study are not adequate to sufficiently assess the test-analysis results.

Vertical drop tests of a composite fuselage section retrofitted with four DEA blocks were conducted to evaluate the performance of the DEA during multi-terrain impact (rigid surface, water, and soft soil). The DEA blocks were designed to limit floor-level accelerations to 20-g. Load attenuation through crushing occurred in both rigid surface and soft soil impacts. In these cases, the impact surface provided adequate reaction load to initiate and maintain stable crushing. Given that the impact velocity conditions were nearly identical, 38.4-

versus 37.4-ft/s, similar acceleration responses were obtained for these two tests. However, for water impact, kinetic energy was dissipated primarily by accelerating the displaced water volume and less than 1-in. of DEA crushing was measured. For all multi-terrain impact tests, measured average floor-level accelerations were below the 20-g limit, thus the design goal of the energy absorber was achieved.

For the rigid surface impact, the Mat 58 model predicted average accelerations 1-g lower than the test range (18.4- to 19.2-g), while the Mat 24 model predicted average accelerations approximately 2-g higher than the test range. Both material models substantially over predicted average floor-level acceleration responses for the water impact test. For the soft-soil impact, both material models predicted similar floor-level acceleration ranges (17.8- to 23.0-g) that were higher than the test values (16.9- to 17.8-g). As stated previously, these simple correlation metrics are insufficient to adequately assess the test-analysis results.

REFERENCES

Aird F. (2006) *Fiberglass & Other Composite Materials: A Guide to Non-Metallic Materials for Race Cars, Street Rods, Body Shops, Boats, and Aircraft*, HPBooks, The Penguin Group, New York, NY.

Baldwin M. (2000) "Final Report – Recommendations for Injury Prevention in Civilian Rotorcraft Accidents," TR-00016, Simula Technologies, Inc., February 29.

Carney K., Melis M., Fasanella E., Lyle K., Gabrys J. (2004) "Material Modeling of Space Shuttle Leading Edge and External Tank Materials for Use in the Columbia Accident Investigation," 8th International LS-DYNA® Users Conference, Dearborn, MI, May 2-4, pp. 3-35 through 3-44.

Fasanella E.L., and Jackson K.E. (2004) "Impact Testing and Simulation of a Crashworthy Composite Fuselage Section with Energy Absorbing Seats and Dummies," *Journal of the American Helicopter Society*, 49 (2), 140-148.

Fasanella E.L. and Kellas S. (2006) "Quasi-Static 3-Point Reinforced Carbon-Carbon Bend Test and Analysis for Shuttle Orbiter Wing Leading Edge Impact Damage Thresholds," NASA Technical Memorandum TM-214505.

Fasanella E.L., Jackson K.E., Lyle K.H., Sparks C.E., and Sareen A. K. (2007) "Multi-Terrain Impact Testing and Simulation of a Composite Energy Absorbing Fuselage Section," *Journal of the American Helicopter Society*, 52 (2), 159-168.

Fasanella E.L., Jackson K.E., and Kellas S. (2008) "Soft Soil Impact Testing and Simulation of Aerospace Structures," Proceedings of the 10th LS-DYNA® Users Conference, Dearborn, MI, June 8-10.

Fasanella E.L., Annett M.S., Jackson K.E., and Polanco M.A. (2012) "Simulating the Response of a Composite Honeycomb Energy Absorber: Part 2. Full-Scale Impact Testing," ASCE 12th Earth and Space Conference, Special Symposium on Ballistic Impact and Crashworthiness, Pasadena, CA, April 15-18.

Hallquist J.Q. (2006) "LS-DYNA® Keyword User's Manual," Volumes I & II, Version 971, Livermore Software Technology Company, Livermore, CA, August.

Jackson K.E. (2001) "Impact Testing and Simulation of a Crashworthy Composite Fuselage Concept," *International Journal of Crashworthiness*, 6 (1), 107-121.

Jackson K.E., Fuchs Y.T., and Kellas S. (2009) "Overview of the NASA Subsonic Rotary Wing Aeronautics Research Program in Rotorcraft Crashworthiness," *Journal of Aerospace Engineering*, 22 (3), 229-239.

Kellas, S. (2004) "Deployable Rigid System for Crash Energy Management," U.S. Patent Nos. 6,755,453 on June 29, 2004; 6,976,729 on December 20, 2005; and 7,040,658 on May 9, 2006.

Kellas S. and Jackson K.E. (2007) "Deployable System for Crash-Load Attenuation," Proceedings of the 63rd American Helicopter Society (AHS) Forum, VA Beach, May 1-3.

Kellas S. and Jackson K.E. (2008) "Multi-Terrain Vertical Drop Tests of a Composite Fuselage Section," Proceedings of the 64th American Helicopter Society (AHS) Annual Forum, Montreal, Canada, April 29-May 1.

Kellas S., Jackson, K.E., and Littell, J.D. (2010) "Full Scale Crash Test of a MD-500 Helicopter with Deployable Energy Absorbers," Proceedings of the 66th American Helicopter Society Forum, Phoenix, AZ, May 11-13.

Kohlgruber D., Vigliotti A., Weissberg V., and Bartosch H. (2004) "Numerical Simulation of a Composite Helicopter Sub-Floor Structure Subjected to Water Impact," Proceedings of the 60th American Helicopter Society Forum, Baltimore, MD, June 7-10.

Littell J. D., Jackson K. E., and Kellas S. (2010) "Crash Test of an MD-500 Helicopter with a Deployable Energy Absorber Concept," Proceedings of the International Crashworthiness Conference, Leesburg, VA, September 22-24.

Lyle K.H., Bark L.W., and Jackson K.E. (2002) "Evaluation of Test/Analysis Correlation Methods for Crash Applications," *Journal of the American Helicopter Society*, 47(4), 219-232.

Matzenmiller A., Lubliner J., and Taylor R. (1995) "A Constitutive Model for Anisotropic Damage in Fiber Composites," *Mechanica of Materials*, 20, 125-152.

Mongiardini M., Ray M.H., Anghileri M. (2009) "Development of a Software for the Comparison of Curves During the Verification and Validation of Numerical Models," Proceedings of the 7th European LS-DYNA Conference, Salzburg, Austria, May 14-15.

Pentecote N. and Kindervater C. M. (2002) "Airframe Water Impact Analysis Using a Local/Global Methodology," Proceedings of the AHS Forum 58, Montreal, Canada, June 11-13.

Polanco M. A., Kellas S., and Jackson K. E. (2009) "Evaluation of Material Models within LS-DYNA® for a Kevlar®/Epoxy Composite Honeycomb," Proceedings of the 65th AHS Forum, Grapevine, TX, May 27-29.

SAE (1995) Society of Automotive Engineers, "Recommended Practice: Instrumentation for Impact Test - Part 1, Electronic Instrumentation," SAE J211/1, March.

Sareen A.K., Sparks C.E., Mullins B.R., Fasanella E.L., and Jackson K.E. (2002) "Comparison of Soft Soil and Hard Surface Impact Performance of a Crashworthy Composite Fuselage Concept," Proceedings of the AHS Forum 58, Montreal, Canada, June 11-13.

Schweizerhof K., Weimar K., Munz Th., and Rottner, Th. (1998) "Crashworthiness Analysis with Enhanced Composite Material Models in LS-DYNA® – Merits and Limits," Proceedings of the 5th International LS-DYNA® Users Conference, Dearborn, Michigan, September 21-22.

Schwer L.E. (2007) "Validation metrics for response histories: perspectives and case studies," *Engineering with Computer*, 23, 295-309.

Tho C.H., Sparks C.E., and Sareen A.K. (2004) "Hard Surface and Water Impact Simulations of Two Helicopter Sub-Floor Concepts," Proceedings of the 60th Forum of the American Helicopter Society, Baltimore, MD, June 7-10.

Vassilakos G. J. *et al.* (2011) "Orion Crew Module Landing System Simulation and Verification," Proceedings of the IEEE Aerospace Conference, Big Sky, Montana.

Witlin G., Smith M., and Richards M. (1997) "Airframe Water Impact Analysis Using a Combined MSC/DYTRAN-DRI/KRASH Approach," Proceedings of the 53rd American Helicopter Society Forum, Virginia Beach, VA, April 29 – May 1.